AGU PUBLICATIONS

JGR

Journal of Geophysical Research: Space Physics

RESEARCH ARTICLE
10.1002/2015JA022169

Key Points:
- EIA impacts the summer-to-winter wind through plasma-neutral collisional heating and ion drag
- The wind is suppressed in summer but accelerates in winter producing large O/N_2 as it converges
- This EIA effect is stronger near December than June causing larger O/N_2 in the northern winter

Correspondence to:
L. Qian,
lqian@ucar.edu

Citation:
Qian, L., A. G. Burns, W. Wang, S. C. Solomon, Y. Zhang, and V. Hsu (2016), Effects of the equatorial ionosphere anomaly on the interhemispheric circulation in the thermosphere, *J. Geophys. Res. Space Physics*, *121*, doi:10.1002/2015JA022169.

Received 13 NOV 2015
Accepted 13 FEB 2016
Accepted article online 18 FEB 2016

Effects of the equatorial ionosphere anomaly on the interhemispheric circulation in the thermosphere

Liying Qian[1], Alan G. Burns[1], Wenbin Wang[1], Stanley C. Solomon[1], Yongliang Zhang[2], and V. Hsu[3]

[1]High Altitude Observatory, National Center for Atmospheric Research, Boulder, Colorado, USA, [2]Applied Physics Laboratory, The Johns Hopkins University, Laurel, Maryland, USA, [3]Department of Aerospace Engineering Sciences, University of Colorado Boulder, Boulder, Colorado, USA

Abstract We investigate the interhemispheric circulation at the solstices, in order to understand why O/N_2 is larger in the northern hemisphere winter than in the southern hemisphere winter. Our studies reveal that the equatorial ionosphere anomaly (EIA) significantly impacts the summer-to-winter wind through plasma-neutral collisional heating, which changes the summer-to-winter pressure gradient, and ion drag. Consequently, the wind is suppressed in the summer hemisphere as it encounters the EIA but accelerates after it passes the EIA in the winter hemisphere. The wind then converges due to an opposing pressure gradient driven by Joule heating in auroral regions and produces large O/N_2 at subauroral latitudes. This EIA effect is stronger near the December solstice than near the June solstice because the ionospheric annual asymmetry creates greater meridional wind convergence near the December solstice, which in turn produces larger O/N_2 in the northern hemisphere winter than in the southern hemisphere winter.

1. Introduction

Thermospheric composition, represented here by the ratio of atomic oxygen to molecular nitrogen (O/N_2), is critical to understanding both the thermosphere and ionosphere. Thermospheric composition drives many well-known coherent phenomena in the thermosphere and ionosphere, both climatologically and during storms. Variations of thermospheric composition during geomagnetic storms are closely related to both positive and negative storm time responses in the ionosphere [e.g., *Mayr et al.*, 1978; *Burns et al.*, 1991, 1995; *Fuller-Rowell et al.*, 1994; *Prölss*, 1993; *Wang et al.*, 2010] and associated mass density variations [*Sutton et al.*, 2005]. Climatologically, thermospheric composition exhibits annual and semiannual variations in which O/N_2 maximizes near equinoxes, with a primary low near the June solstice and a secondary low near the December solstice [e.g., *Qian et al.*, 2009]. This annual/semiannual variation of thermospheric composition contributes to annual and semiannual variations in thermospheric mass density [e.g., *Fuller-Rowell*, 1998; *Qian et al.*, 2009; *Qian and Solomon*, 2012]. In the ionosphere, annual/semiannual variation of O/N_2 is the main forcing that drives annual and semiannual variations in daytime N_mF_2 at low and middle latitudes [e.g., *Torr and Torr*, 1973; *Rishbeth*, 1998; *Rishbeth et al.*, 2000; *Burns et al.*, 2012; *Qian et al.*, 2013].

In this paper, we focus on thermospheric composition variations during the June and December solstices. At the solstices, O/N_2 shows a seasonal variation in which O/N_2 is larger in the winter hemisphere than that in the summer hemisphere [e.g., *Hedin et al.*, 1974; *Jacchia*, 1974; *Mayr et al.*, 1978]. In the ionosphere, this seasonal variation of O/N_2 is found to be closely related to the winter anomaly of N_mF_2, which is defined as occurring when daytime N_mF_2 is larger in the winter hemisphere than it is in the conjugate summer hemisphere at middle latitudes [e.g., *Torr and Torr*, 1973; *Rishbeth*, 1998; *Burns et al.*, 2014].

Recent O/N_2 data observed by the Global Ultraviolet Imager (GUVI) on board the Thermosphere-Ionosphere Mesosphere Energetics Dynamics (TIMED) satellite reveal that the summer-winter seasonal variation of O/N_2 exhibits a hemispheric asymmetry, with larger O/N_2 in the northern hemisphere winter compared to that in the southern hemisphere winter [e.g., *Qian et al.*, 2009; *Burns et al.*, 2014]. This hemispheric asymmetry of O/N_2 is consistent with a hemispheric asymmetry of the ionospheric winter anomaly, as the ionospheric winter anomaly is stronger in the Northern Hemisphere than in the Southern Hemisphere. *Torr and Torr* [1973] found that the ionospheric winter anomaly occurred more often and was stronger in the northern hemisphere than in the southern hemisphere; they also found that this hemispheric asymmetry of the winter

anomaly seemed to be closely related to O/N_2. *Burns et al.* [2014] found that there is a greater winter increases in electron density in the Northern Hemisphere than in the Southern Hemisphere, and this hemispheric asymmetry of the winter anomaly appears to be related to the greater seasonal variation of O/N_2 in the Northern Hemisphere, compared to the Southern Hemisphere. Clearly, understanding the hemispheric asymmetry of the seasonal variation of O/N_2 is a key to understand the hemispheric asymmetry of the ionospheric winter anomaly. The question is, why does the summer-winter seasonal variation of thermospheric composition exhibit a hemispheric asymmetry? It is important to note that since the F_2 layer peak (h_mF_2) tends to remain on a fixed pressure surface, and N_mF_2 is proportional to O/N_2 [*Rishbeth*, 1998], thus, we are interested in composition on fixed pressure surfaces in this paper.

Seasonal variation of thermospheric composition has been attributed to the large-scale interhemispheric circulation [e.g., *Mayr et al.*, 1978; *Burns et al.*, 1989; *Rishbeth*, 1998; *Rishbeth and Müller-Wodarg*, 1999]. Thermospheric composition can also vary responding to temperature variations through thermal expansion and contraction, but this change of composition only occurs at a fixed altitude and composition at a fixed pressure surface remains unchanged [*Burns et al.*, 1995]. Dynamical upwelling and downwelling are the primary driver for composition change on a fixed pressure surface [*Burns et al.*, 1989; *Rishbeth*, 1998]. At solstices, larger solar heating in the summer hemisphere, compared to the winter hemisphere, drives a prevailing (daily average) summer-to-winter, large-scale circulation in the middle and upper thermospheres and a small return flow from the winter hemisphere to the summer hemisphere in the lower thermosphere, with upwelling in the summer hemisphere and downwelling in the winter hemisphere.

The thermosphere is diffusively separated, with heavier species dominant at lower altitudes and lighter species dominant at higher altitudes. Therefore, upwelling in the summer hemisphere transports heavier species from the lower thermosphere upward and increases the relative abundance of heavier species at a particular pressure surface. Downwelling in the winter hemisphere transports lighter species downward and increases the relative abundance of lighter species at a fixed pressure surface. Therefore, in order to understand the hemispheric asymmetry of the high O/N_2 in the winter hemispheres, we need to understand the interhemispheric circulations at the solstices.

In this paper, we will investigate the interhemispheric circulations at the solstices. We will conduct modeling studies to examine differences of the interhemispheric wind circulation during these two periods, the mechanisms that determine these differences, and how these differences determine the hemispheric asymmetry of the summer-to-winter variation of thermospheric composition, and thus, the hemispheric asymmetry of the ionosphere winter anomaly. O/N_2 observed by the TIMED/GUVI will be used to verify and illustrate the hemispheric asymmetry of the seasonal variation of thermospheric composition. The model we will use is the National Center for Atmospheric Research (NCAR) Thermosphere-Ionosphere-Electrodynamics General Circulation Model (TIE-GCM) [*Qian et al.*, 2012].

2. O/N_2 Data From TIMED/GUVI and Model Description

The TIMED/GUVI measures airglow emissions from H, O, and N_2 and absorption by O_2, in the spectral range from 120 to 180 nm [*Christensen et al.*, 2003]. The sunlit disk emission measurements of the atomic oxygen emission at 135.6 nm (OI 135.6 nm) and N_2 LBH molecular bands (141 to 153 nm) are used to derive column number density ratio O/N_2 above an altitude where the N_2 column density is $10^{17}\,cm^{-2}$ (approximately 140 km) [*Zhang et al.*, 2004]. In this study we used TIMED/GUVI data from 2002 to 2007; the data in 2003 are shown to illustrate the O/N_2 distribution at the solstices near solar maximum.

The NCAR TIE-GCM is a first-principles upper atmosphere general circulation model that solves the Eulerian continuity, momentum, and energy equations for the coupled thermosphere/ionosphere system. It utilizes latitude and longitude as the horizontal coordinates and pressure surfaces as the vertical coordinate. The pressure interfaces are defined as $z = \ln(P_0/P)$, where P_0 is a reference pressure of 5×10^{-4} μb. The vertical range of the pressure interfaces is from −7 to 7, which covers an altitude range about 97–600 km depending on solar activity [*Roble et al.*, 1988; *Richmond et al.*, 1992; *Qian et al.*, 2012]. In this study, we utilize the standard version of the model, which has a horizontal resolution of $5° \times 5°$ and a vertical resolution of one half pressure scale height. A detailed description of the model is given by *Qian et al.* [2012] and will not be repeated here.

3. Methodology

We ran NCAR TIE-GCM for January and July 2003. The year 2003 was near solar maximum, and TIMED/GUVI measurements of O/N_2 were available. We examine monthly and zonal mean, daily averaged values of important state variables in the coupled thermosphere-ionosphere system. These include temperature, winds, O/N_2, and electron density. We also investigate the energetics in the thermal energy equation and the forces in the meridional momentum equation, focusing on differences in the summer-to-winter circulation in January and July that might cause the hemispheric asymmetry of the seasonal variation of thermospheric composition. This enables us to determine the mechanisms that drive these differences. We investigate monthly mean quantities to smooth out day-to-day variability to look at the prevailing behavior in each season. The monthly mean values for $F_{10.7}$ and *Kp*, obtained from the NOAA Space Physics Interactive Data Resource (SPIDR), were 140 and 2.4, respectively, in January 2003. They were 134 and 2.9, respectively, in July 2003. Therefore, the solar conditions and geomagnetic activity levels in January 2003 were close to those in July 2003; thus, geomagnetic activity should not have a large effect on our results.

4. Results

During the solstices, the summer-to-winter meridional wind blows through the equatorial ionization anomaly (EIA) region, which is characterized by enhanced electron densities on each side of the magnetic equator. The EIA is strongly coupled to the thermosphere energetically through plasma-neutral collisions, which heat the neutral atmosphere, and dynamically through ion drag, which exerts a drag force on the meridional wind. Therefore, questions arise as to how the EIA affects the prevailing summer-to-winter wind and whether these effects could be different in January and July. We answer these questions using modeling studies in this section. We conducted an analysis of the modeling results in both the geographic and geomagnetic coordinates. Both analyses arrived at the same conclusions regarding the EIA effect on the summer-to-winter meridional circulation. However, since the EIA and its associated processes are better defined in geomagnetic coordinates, we show modeling results in these coordinates.

Figure 1 shows monthly and zonal mean, daily averaged electron density, neutral heating due to plasma-neutral collisions, and the meridional temperature gradient, defined as $\Delta T = T_{j2} - T_{j1}$, where T_{j1} and T_{j2} are the temperatures at two consecutive latitudes (5° apart) from left to right on the *x* axis. All quantities are shown as daily averaged values to be consistent with the prevailing summer-to-winter wind, which is a daily averaged quantity. The *y* axis is model pressure levels from 0 to 7, which corresponds to the *F* region ionosphere, covering an altitude range from ~200 km to ~600 km. The *x* axis shows the geomagnetic latitudes. Note that the *x* axes for both January (left column) and July (right column) are from the summer hemisphere on the left side to the winter hemisphere on the right hand side, for easier comparisons between January and July.

The EIA in January is stronger than that in July (Figure 1). This is the ionosphere annual asymmetry in the F_2 layer in which average F_2 layer electron densities are larger near the December solstice than they are near the June solstice [e.g., *Rishbeth and Müller-Wodarg*, 2006; *Zeng et al.*, 2008]. Since the EIA is stronger in January, neutral heating through plasma-neutral collisions (Q_{eni}) is also larger in January than in July, as shown in Figure 1. This neutral heating, which is the dominant neutral heating process near and above the F_2 peak, modifies the solar heating-induced, summer-to-winter temperature gradient. For example, the temperature gradients diminish in the ~0°–30° region and are enhanced again in the ~30°–60° region in the winter hemisphere, due to EIA heating, and this modification is larger in January than in July. Temperature gradients in the high-latitude regions are small or even positive, due to high-latitude heating that was driven by geomagnetic activity (in both the summer and winter hemispheres) and solar heating (in the summer hemisphere). This paper does not address these high-latitude processes. Therefore, we will only briefly mention the high-latitude regions when necessary.

The modification of the temperature gradient by the EIA heating changes the pressure gradient. Figure 2 has the same *x* axis and *y* axis as Figure 1 does. Figure 2 (top row) shows monthly and zonal mean, diurnally averaged, meridional pressure gradients for January and July. Due to the heating near the EIA, the pressure gradients have a peak on each side of the equator, separated by a minimum pressure gradient region in the low-latitude region in winter. This is different from the situation that would occur if solar heating alone caused these pressure gradients. In that case the pressure gradients would be controlled by solar zenith angle.

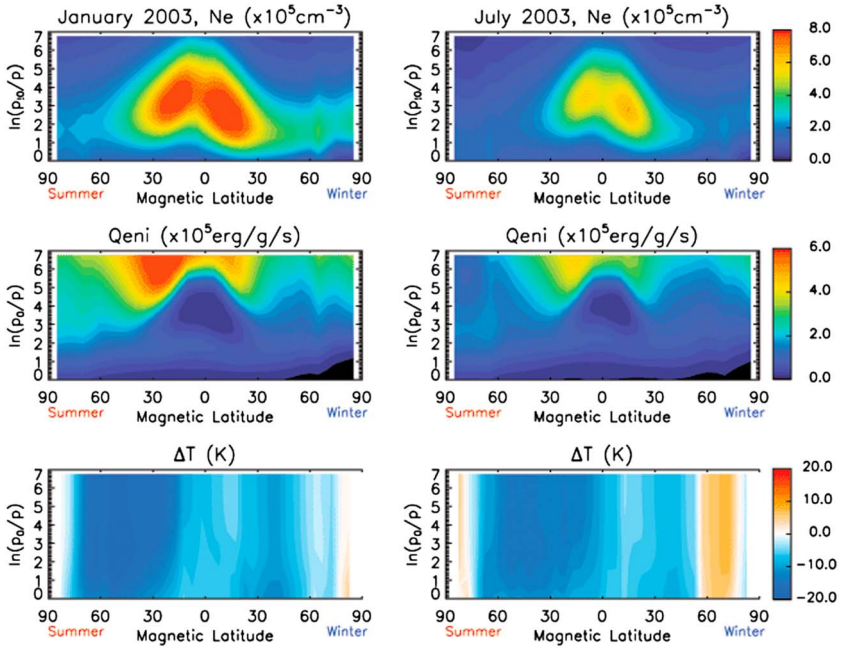

Figure 1. (top row) Monthly and zonal mean, daily averaged, electron density, (middle row) neutral heating by plasma-neutral collisions, and (bottom row) the neutral temperature gradient. (left column) January 2003 and (right column) July 2003. The *y* axes are model pressure levels, the *x* axes are equivalent to geomagnetic latitudes, but with the summer hemisphere on the left side and the winter hemisphere on the right side. The start location of the differencing for the temperature gradients is at −87.5° and 87.5° magnetic latitudes for January and July, respectively.

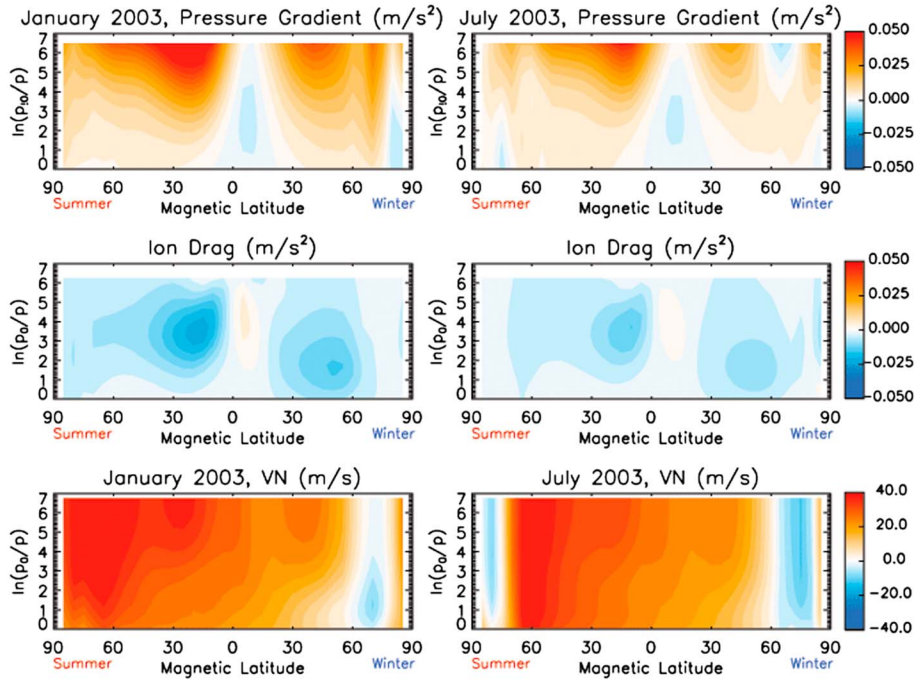

Figure 2. (top row) Monthly and zonal mean, daily averaged, meridional pressure gradient, (middle row) meridional ion drag, and (bottom row) meridional neutral wind. (left column) January 2003 and (right column) July 2003. The *y* axes are model pressure levels, the *x* axes are equivalent to geomagnetic latitudes, but with the summer hemisphere on the left side and the winter hemisphere on the right side.

Therefore, they would be more or less continuous across the equatorial area. In January, stronger neutral heating near the winter EIA (~0°–30°, Q_{eni} in Figure 1) causes a stronger pressure gradient in the winter midlatitudes (~30°–60°, Figure 2). In this paper, we focus on this winter midlatitude region since this is the region associated with the large winter O/N_2 that contributes to the ionosphere winter anomaly.

There are other forces that contribute to the strength of the meridional wind. According to the momentum equation, meridional wind is determined by pressure gradient, ion drag, Coriolis force, horizontal advection, vertical advection, viscosity, and horizontal diffusion. We investigated the rest of the forces simulated by the model and found that vertical advection, viscosity, and horizontal diffusion are secondary compared to other forces. Horizontal advection is important at high latitudes where there are both strong winds and horizontal gradients of winds [*Wang et al.*, 2008]. Ion drag can be an important mechanism through which the EIA can affect the summer-to-winter wind dynamically. Figure 2 (middle row) shows the meridional ion drag for January and July. Ion drag by the summer EIA is larger in January than in July, due to the larger electron density in January (Figure 1). Ion drag in the winter EIA is near zero for both January and July since meridional ion drift is in the same direction as the neutral meridional wind in this hemisphere, whereas it is in the opposite direction in the summer hemisphere. At midlatitudes (~30°–60°), ion drag is also larger in January than in July, due to the ionosphere annual asymmetry, which results in larger midlatitude electron density in January.

Figures 2 (top and middle rows) and 1 (top and middle rows) indicate that the EIA can have a strong effect on the summer-to-winter wind through both ion drag and plasma-neutral heating. Figure 2 (bottom row) shows meridional winds (VN) for January and July. The winter EIA heating causes a wind peak at midlatitudes in the winter hemisphere, which is stronger in January than in July due to the stronger winter EIA heating in January. The strength of the summer-to-winter wind in the winter midlatitude region is important since it largely determines the convergence and thus the strength of downwelling in the subauroral region in the winter hemisphere, which in turn controls O/N_2 in this region.

Figure 3 shows wind vectors overplotted on contours of electron density (top row) and the natural logarithm of O/N_2 (bottom row). The wind vectors are those of the meridional wind and vertical wind, with the vertical wind multiplied by 100 to be compatible with the meridional wind in magnitude. Figure 3 is in the same style as Figures 1 and 2. The wind vectors in black indicate the upward vertical wind, whereas those in white indicate the downward vertical wind. There are two convergence zones (regions of downward winds), one in the magnetic equator region after the meridional wind passes the summer EIA and before it encounters the winter EIA, the other in the ~30°–60° (subauroral) region after the meridional wind passes the winter EIA and before it encounters Joule heating in the auroral regions. The Joule heating in the auroral regions weakens the summer-to-winter pressure gradient or even reverses the pressure gradient. In both regions, the convergences are stronger in January due to the stronger EIA heating (Figure 1). Note that there are divergences (upward vertical winds) at high latitudes in both January and July, due to high-latitude heating that was driven by geomagnetic activity (in both the summer and winter hemispheres) and solar heating (in the summer hemisphere). These divergences decrease O/N_2 in these high-latitude regions, as seen in Figure 3. During strong geomagnetic storms, the decrease of O/N_2 due to high-latitude Joule heating can extend to middle and low latitudes. The effect of high-latitude processes on thermospheric composition is an interesting topic itself, but it is beyond the scope of this paper. Therefore, we will not discuss these high-latitude regions further.

In January, the stronger meridional wind in the winter midlatitude region (Figure 2) causes a stronger convergence, and thus stronger downwelling in the subauroral region (Figure 3), compared with July. Since the main cause of the summer-to-winter composition variability is vertical advection [e.g., *Burns et al.*, 1989; *Rishbeth*, 1998; *Rishbeth and Müller-Wodarg*, 1999], O/N_2, as well as the latitudinal gradient of O/N_2, is larger in this region in January than in July. Note that vertical advection is the multiplication of vertical wind and vertical gradient of O/N_2 (with respect to pressure surfaces); therefore, both the vertical wind and the vertical gradient of O/N_2 contribute to the value of O/N_2 [*Burns et al.*, 2015]. Here in the subauroral region in the winter hemisphere, both the vertical wind (Figure 3) and the vertical gradient of O/N_2 (not shown) are larger in January than in July. Also note that in the summer hemisphere, the summer EIA heating should weaken the solar heating-induced summer-to-winter temperature gradient, which in turn reduces the summer-to-winter meridional wind. The ion drag in the summer EIA region also reduces the summer-to-winter meridional wind. Therefore, the EIA has the effect of suppressing vertical advection in the summer. Since vertical advection in

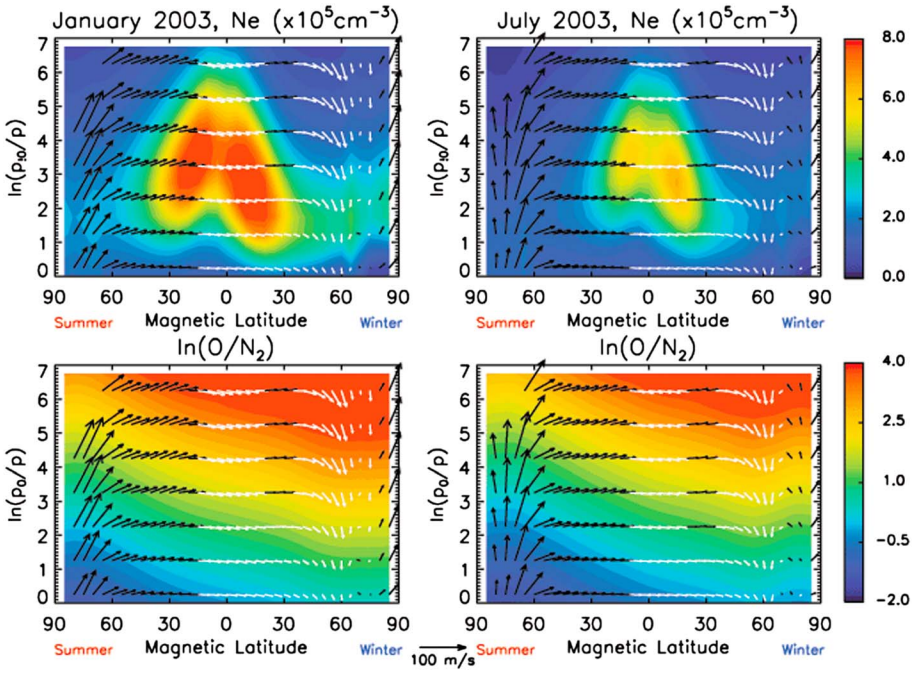

Figure 3. (top row) Monthly and zonal mean, daily averaged, electron density and (bottom row) natural logarithm of (O/N_2). Overplotted are vectors of the meridional wind and vertical wind, with the vertical wind multiplied by 100 to be compatible with the meridional wind in magnitude. Black wind vectors indicate upward vertical wind, whereas white wind vectors indicate downward vertical wind. (left column) January 2003 and (right column) July 2003. The *y* axes are model pressure levels, the *x* axes are equivalent to geomagnetic latitudes, but with the summer hemisphere on the left side and the winter hemisphere on the right side.

the summer hemisphere reduces O/N_2, the EIA effectively increases O/N_2 in the summer hemisphere. This effect, reflected in O/N_2 in the summer hemisphere, should be stronger in January than in July, due to the stronger heating and ion drag in the January summer hemisphere (Figure 1).

The aforementioned effect of the EIA on the summer-to-winter meridional wind, and consequently, its influence on O/N_2, especially in the winter hemisphere, can be verified and illustrated using O/N_2 measured by the TIMED/GUVI. Figure 4 shows January and July median O/N_2 measured by TIMED/GUVI and simulated by the NCAR TIE-GCM, in geographic coordinates. Due to orbital precession, local times of TIMED/GUVI O/N_2 observations changed from 15:43 to 09:27 in January and from 16:10 to 09:55 in July, respectively. Therefore, the observational local times in January are very similar to those in July, so local time effects should be minimal. The simulated O/N_2 was sampled the same way as the data. There are no data at high latitudes beyond ~60° in the winter hemisphere since TIMED/GUVI can only measure O/N_2 in sunlit conditions. TIMED/GUVI O/N_2 shows the following features: (1) midlatitude O/N_2 in the January winter hemisphere (Northern Hemisphere) is much larger than that in the July winter hemisphere (Southern Hemisphere); (2) the latitudinal gradient of O/N_2 is larger in January than in July; (3) zonal mean O/N_2 in the January summer hemisphere is slightly larger than the zonal mean O/N_2 at equivalent latitudes in the July summer hemisphere; and (4) consequently, O/N_2 is larger in January than in July on a global average basis. These features are true for all the years from 2002 to 2007 in TIMED/GUVI O/N_2. Aspects (1)–(3) largely drive the hemispheric differences in the ionosphere winter anomaly in daytime N_mF_2 [*Rishbeth*, 1998], whereas aspect (4) is largely caused by the ionosphere's annual asymmetry in the F_2 layer but should also have feedback effects on the ionosphere's annual asymmetry, considering that O/N_2 is closely related to N_mF_2 [*Rishbeth*, 1998]. The main discrepancy between the data and the model results occurs at high latitudes in the summer hemisphere, where the simulated O/N_2 is larger than the data. However, model results clearly shows features that are consistent with the EIA effect on the summer-to-winter meridional circulation, with larger O/N_2 in the northern winter hemisphere (January) than in the southern winter hemisphere (July).

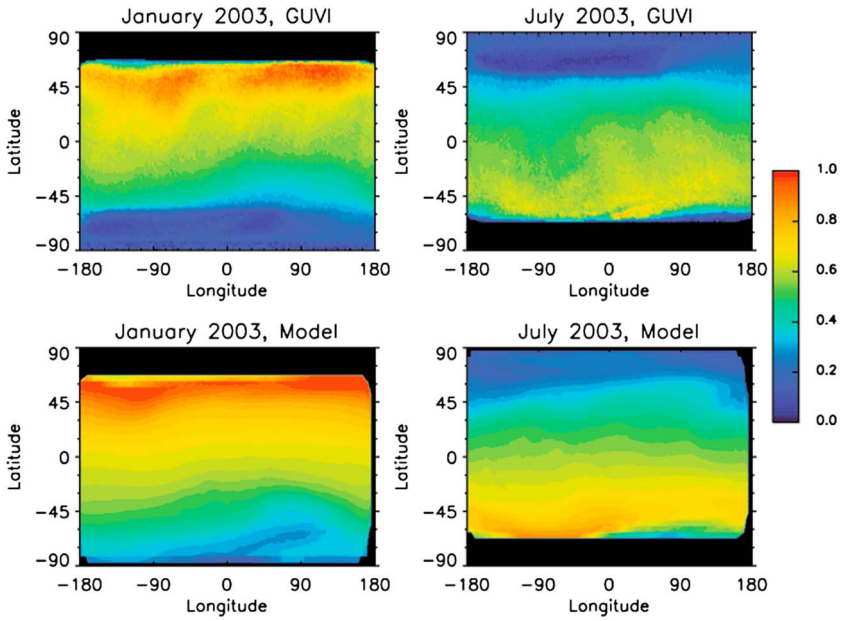

Figure 4. O/N_2 observed by TIMED/GUVI and simulated by NCAR TIE-GCM. (left) Median O/N_2 in January 2003 and (right) median O/N_2 in July 2003. Solar local times for January changed from 15:43 to 09:27 due to orbit precession, whereas they changed from 16:10 to 09:55 for July.

5. Conclusions and Discussion

In this paper, we investigated the large-scale, interhemispheric meridional wind at the solstices, driven by the need to understand the hemispheric asymmetry of the summer-winter seasonal variation of thermospheric composition (O/N_2) and N_mF_2. This hemispheric asymmetry in composition is defined as a larger O/N_2 in the northern hemisphere winter than in the southern hemisphere winter. We conducted NCAR TIE-GCM model simulations for January and July of 2003, which have similar monthly mean solar and geomagnetic conditions. We analyzed monthly and zonal mean, diurnally averaged quantities of the thermosphere and ionosphere key state variables including temperatures, winds, O/N_2, and electron density; energetics; and forces in the meridional momentum equation. Our findings are as follows:

1. The EIA interrupts the solar heating-induced, summer-to-winter meridional wind. This interruption is primarily due to plasma-neutral collisional heating, which maximizes near the EIA. This EIA-associated heating counteracts the summer-to-winter pressure gradient in the summer hemisphere but increases pressure gradients in the winter hemisphere. As a result, instead of exhibiting a morphology influenced by solar zenith angles, pressure gradients have a peak on each side of the equator, separated by a minimum pressure gradient region in the winterside low latitudes.
2. Consequently, the summer-to-winter wind is suppressed as it encounters the EIA in the summer hemisphere but accelerates again at midlatitudes in the winter hemisphere after it passes through the EIA. The meridional wind then converges as equator-pole pressure gradients diminish at high latitudes and is countered by Joule heating in auroral regions creating an opposing pressure gradient. These convergence and thus downwelling cause large values of O/N_2 at subauroral latitudes in the winter hemisphere.
3. This EIA effect is stronger near the December solstice than near the June solstice. This December/June difference is caused by the ionosphere annual asymmetry: there is more electron density near the December solstice than near the June solstice. As a result, the meridional wind convergence and downwelling at subauroral latitudes in the winter hemisphere are stronger in January than in July. These stronger convergence and hence downwelling lead to a larger O/N_2 in the January winter hemisphere (Northern Hemisphere) than in the July winter hemisphere (Southern Hemisphere), causing the hemispheric asymmetry of the summer-winter seasonal variation of thermospheric composition and consequently in the ionospheric winter anomaly.

4. In the summer hemisphere, ion drag due to the EIA suppresses the meridional wind, which effectively enhances O/N_2. In the winter hemisphere, since the meridional ion drifts are in the same direction as the meridional neutral winds, dynamical influences of the EIA on the summer-to-winter wind, through ion drag, do not play a significant role in influencing thermosphere composition in the winter hemisphere.

This effect of the EIA on the interhemispheric circulation can be an important mechanism for the vertical coupling between the lower atmosphere and the upper atmosphere: upward propagating waves, such as tides, influence ion drift in the EIA region through the neutral wind dynamo and thus changes the EIA; the EIA then affects the interhemispheric circulation through ion drag and plasma-neutral collisional heating, which then changes the meridional wind, particularly, the convergence and downwelling at midlatitudes in the winter hemisphere, and consequently, thermosphere composition and the ionosphere. For example, observational and modeling studies have found that sudden stratospheric warming (SSW) influence the upper atmosphere [e.g., *Liu and Roble*, 2002; *Goncharenko et al.*, 2010]. This chain of processes could be a pathway through which the SSW affects the middle and high latitudes of the upper atmosphere.

Note that in this paper, we have been concerned with the average seasonal behavior near the two solstices. To do this, we have examined all quantities as monthly means. There will also be day-to-day variability depending on solar and geomagnetic conditions, as well as internal thermospheric conditions. For example, the relative strength of the meridional wind and high-latitude Joule heating in the winter hemisphere determines the latitudes and magnitudes of convergence and downwelling. In addition, we examined the EIA effects on a zonal mean basis. The EIA should have longitudinal variability due the positions of the magnetic poles, which can affect the ionosphere as well as the thermosphere, and thus the effects of the EIA on the meridional wind and thermospheric composition. Furthermore, this EIA effect could have a solar cycle variation, which can at least affect the solar cycle variability of the ionosphere winter anomaly [e.g., *Torr and Torr*, 1973; *Burns et al.*, 2014]. The longitudinal and solar cycle variabilities of the EIA effect on the meridional wind and thermospheric composition will be reported in separate papers.

Acknowledgments

This research was supported by NASA grant NNX12AJ54G from the NASA Guest Investigator Program and NASA LWS grants NNX10AQ59G, NNX14AE06G, NNX15AB83G, and NNX13AE20G to the National Center for Atmospheric Research; and NASA GOLD contract NNG12PQ28C to the University of Central Florida. We would like to thank the TIMED/GUVI team for the O/N_2 measurements, and the NOAA Space Physics Interactive Data Resource (SPIDR) for the *Kp* and $F_{10.7}$ indices. TIMED/GUVI is supported by NASA grant NNX12AG45G. NCAR is sponsored by the National Science Foundation. All data that produced the results in this paper are available on NCAR's High Performance Storage System upon request.

References

Burns, A. G., T. L. Killeen, and R. G. Roble (1989), Processes responsible for the compositional structure of the thermosphere, *J. Geophys. Res.*, *94*, 3670–3686, doi:10.1029/JA094iA04p03670.

Burns, A. G., T. L. Killeen, and R. G. Roble (1991), A theoretical study of thermospheric composition perturbations during an impulsive geomagnetic storm, *J. Geophys. Res.*, *96*, 14,153–14,167, doi:10.1029/91JA00678.

Burns, A. G., T. L. Killeen, W. Deng, G. R. Carignan, and R. G. Roble (1995), Geomagnetic storm effects in the low- to middle-latitude upper thermosphere, *J. Geophys. Res.*, *100*, 14,673–14,691, doi:10.1029/94JA03232.

Burns, A. G., S. C. Solomon, W. Wang, L. Qian, Y. Zhang, and L. J. Paxton (2012), Daytime climatology of ionospheric N_mF_2 and h_mF_2 from COSMIC data, *J. Geophys. Res.*, *117*, A09315, doi:10.1029/2012JA017529.

Burns, A. G., W. Wang, L. Qian, S. C. Solomon, Y. Zhang, L. J. Paxton, and X. Yue (2014), On the solar cycle variation of the winter anomaly, *J. Geophys. Res. Space Physics*, *119*, 4938–4949, doi:10.1002/2013JA019552.

Burns, A. G., S. C. Solomon, W. Wang, L. Qian, Y. Zhang, L. J. Paxton, X. Yue, J. P. Thayer, and H. L. Liu (2015), Explaining solar cycle effects on composition as it relates to the winter anomaly, *J. Geophys. Res. Space Physics*, *120*, 5890–5898, doi:10.1002/2015JA021220.

Christensen, A. B., et al. (2003), Initial observations with the Global Ultraviolet Imager (GUVI) in the NASA TIMED satellite mission, *J. Geophys. Res.*, *108*(A12), 1451, doi:10.1029/2003JA009918.

Fuller-Rowell, T. J. (1998), The "thermospheric spoon": A mechanism for the semiannual density variation, *J. Geophys. Res.*, *103*, 3951–3956, doi:10.1029/97JA03335.

Fuller-Rowell, T. J., M. V. Codrescu, R. J. Moffett, and S. Quegan (1994), Response of the thermosphere and ionosphere to geomagnetic storms, *J. Geophys. Res.*, *99*, 3893–3914, doi:10.1029/93JA02015.

Goncharenko, L. P., A. J. Coster, J. L. Chau, and C. E. Valladares (2010), Impact of sudden stratospheric warmings on equatorial ionization anomaly, *J. Geophys. Res.*, *115*, A00G07, doi:10.1029/2010JA015400.

Hedin, A. E., H. G. Mayr, C. A. Reber, and N. W. Spencer (1974), Empirical model of global thermospheric temperature and composition based on data from the OGO 6 quadruple mass spectrometer, *J. Geophys. Res.*, *79*, 215–225, doi:10.1029/JA079i001p00215.

Jacchia, L. G. (1974), Variations in thermospheric composition: A model based on mass spectrometer and satellite drag data, *J. Geophys. Res.*, *79*, 1923–1927, doi:10.1029/JA079i013p01923.

Liu, H. -L., and R. G. Roble (2002), A study of a self-generated stratospheric sudden warming and its mesospheric/lower thermospheric impacts using coupled TIME-GCM/CCM3, *J. Geophys. Res.*, *107*(D23), 4695, doi:10.1029/2001JD001533.

Mayr, H. G., I. Harris, and N. W. Spencer (1978), Some properties of upper dynamics, *Rev. Geophys.*, *16*, 539–565, doi:10.1029/RG016i004p00539.

Prölss, G. W. (1993), Common origin of positive ionospheric storms at middle latitudes and the geomagnetic activity effect at low latitudes, *J. Geophys. Res.*, *98*, 5981–5991, doi:10.1029/92JA02777.

Qian, L., and S. C. Solomon (2012), Thermospheric density: An overview of temporal and spatial variations, *Space Sci. Rev.*, *168*, 147–173, doi:10.1007/s11214-011-9810-z.

Qian, L., S. C. Solomon, and T. J. Kane (2009), Seasonal variation of thermospheric density and composition, *J. Geophys. Res.*, *114*, A01312, doi:10.1029/2008JA013643.

Qian, L., A. G. Burns, B. A. Emery, B. Foster, G. Lu, A. Maute, A. D. Richmond, R. G. Roble, S. C. Solomon, and W. Wang (2012), The NCAR TIE-GCM: A community model of the coupled thermosphere/ionosphere system, *Am. Geophys. Monogr.*, doi:10.1029/2012GM001297.

Qian, L., A. G. Burns, S. C. Solomon, and W. Wang (2013), Annual/semiannual variation of the ionosphere, *Geophys. Res. Lett.*, *40*, 1928–1933, doi:10.1002/grl.50448.

Richmond, A. D., E. C. Ridley, and R. G. Roble (1992), A thermosphere/ionosphere general circulation model with coupled electrodynamics, *Geophys. Res. Lett.*, *19*, 601–604, doi:10.1029/92GL00401.

Rishbeth, H. (1998), How the thermospheric circulation affects the ionospheric F_2-layer, *J. Atmos. Sol. Terr. Phys.*, *60*, 1385–1402.

Rishbeth, H., and I. C. F. Müller-Wodarg (1999), Vertical circulation and thermospheric composition: A modelling study, *Ann. Geophys.*, *17*, 794–805.

Rishbeth, H., and I. C. F. Müller-Wodarg (2006), Why is there more ionosphere in January than in July? The annual asymmetry in the F_2-layer, *Ann. Geophys.*, *24*, 3293.

Rishbeth, H., I. C. F. Müller-Wodarg, L. Zou, T. J. Fuller-Rowell, G. H. Millward, R. J. Moffett, D. W. Idenden, and A. D. Aylwardm (2000), Annual and semiannual variations in the ionospheric F_2-layer: II. Physical discussion, *Ann. Geophys.*, *18*, 945–956.

Roble, R. G., E. C. Ridley, A. D. Richmond, and R. E. Dickinson (1988), A coupled thermosphere/ionosphere general circulation model, *Geophys. Res. Lett.*, *15*, 1325–1328, doi:10.1029/GL015i012p01325.

Sutton, E. K., J. M. Forbes, and R. S. Nerem (2005), Global thermospheric neutral density and wind response to the severe 2003 geomagnetic storms from CHAMP accelerometer data, *J. Geophys. Res.*, *110*, A09S40, doi:10.1029/2004JA010985.

Torr, M. R., and D. G. Torr (1973), The seasonal behaviour of the F_2-layer of the ionosphere, *J. Atmos. Terr. Phys.*, *35*, 2237–2251.

Wang, W., A. G. Burns, M. Wiltberger, S. C. Solomon, and T. L. Killeen (2008), Altitude variations of the horizontal thermospheric winds during geomagnetic storms, *J. Geophys. Res.*, *113*, A02301, doi:10.1029/2007JA012374.

Wang, W., J. Lei, A. G. Burns, S. C. Solomon, M. Wiltberger, J. Xu, Y. Zhang, L. Paxton, and A. Coster (2010), Ionospheric response to the initial phase of geomagnetic storms: Common features, *J. Geophys. Res.*, *115*, A07321, doi:10.1029/2009JA014461.

Zeng, Z., A. Burns, W. Wang, J. Lei, S. Solomon, S. Syndergaard, L. Qian, and Y.-H. Kuo (2008), Ionospheric annual asymmetry observed by the COSMIC radio occultation measurements and simulated by the TIEGCM, *J. Geophys. Res.*, *113*, A07305, doi:10.1029/2007JA012897.

Zhang, Y., L. J. Paxton, D. Morrison, B. Wolven, H. Kil, C.-I. Meng, S. B. Mende, and T. J. Immel (2004), O/N_2 changes during 1–4 October 2002 storms: IMAGE SI-13 and TIMED/GUVI observations, *J. Geophys. Res.*, *109*, A10308, doi:10.1029/2004JA010441.